Self-Assembling Thiophene Dendrimers with a Hexa-peri-hexabenzocoronene Core—Synthesis, Characterization and Performance in Bulk Heterojunction Solar Cells

ARTICLE *in* CHEMISTRY OF MATERIALS · DECEMBER 2009

Impact Factor: 8.35 · DOI: 10.1021/cm903272y

CHEMISTRY OF MATERIALS
Article

Chem. Mater. **2010,** *22,* 457–466 457
DOI:10.1021/cm903272y

Self-Assembling Thiophene Dendrimers with a Hexa-*peri*-hexabenzocoronene Core−Synthesis, Characterization and Performance in Bulk Heterojunction Solar Cells

Wallace W. H. Wong,*[,†] Chang-Qi Ma,[‡] Wojciech Pisula,[§] Chao Yan,[†] Xinliang Feng,[§] David J. Jones,[†] Klaus Müllen,[§] René A. J. Janssen,[⊥] Peter Bäuerle,[‡] and Andrew B. Holmes[†]

[†]*School of Chemistry, Bio21 Institute, University of Melbourne, 30 Flemington Road, Parkville, Victoria 3010, Australia,* [‡]*Institut für Organische Chemie II und Neue Materialien, Universität Ulm, Albert-Einstein-Allee 11, D-89081, Ulm, Germany,* [§]*Max Planck Institute for Polymer Research, Ackermannweg 10, D-55128 Mainz, Germany, and* [⊥]*Molecular Materials and Nanosystems, Eindhoven University of Technology, P.O. Box 513, 5600 MB Eindhoven, The Netherlands*

Received October 26, 2009. Revised Manuscript Received December 8, 2009

The solid state organization of molecules is an important factor in determining the performance of organic electronic devices. In bulk heterojunction (BHJ) solar cells, the arrangement of electron donor and acceptor materials into distinct crystalline phases of ideal size and distribution can lead to better power conversion efficiencies. The use of fluorenyl hexa-*peri*-hexabenzocoronene (FHBC) **2** in this study has highlighted the importance of molecular organization to device performance. FHBC compounds **6**, **8**, and **10**, functionalized with a series of thiophene dendrons, were synthesized using Suzuki−Miyaura coupling in high yields. In UV−vis and ^{1}H NMR spectroscopic studies, all FHBC derivatives showed self-association in solution. Hexagonal packing of columnar structures was observed for solid state samples of FHBC **2** and **8** in two-dimensional wide-angle X-ray scattering experiments. In thin film X-ray experiments, ordered structures were observed in blends of FHBC **2** and fullerene acceptor materials indicating that there is phase separation between the donor and acceptor materials and that the self-organization of the FHBC material is unaffected. While the large thiophene dendritic substituent attached to compound **10** broadened its UV−vis absorption profile, the solid state morphology is altered by the bulky thiophene dendrons. These molecular structure variations are reflected in the performance characteristics of BHJ solar cell devices fabricated using these FHBC compounds as electron donor materials. Power conversion efficiency of 2.5% was achieved for a device containing compound **10** with [6,6]-phenyl-C71-butyric acid methyl ester ($PC_{71}BM$) as the acceptor material. This compares favorably with devices fabricated with pure dendritic thiophene materials and illustrates the positive effect of molecular self-organization on device performance.

Introduction

There are numerous criteria for the design of molecules for application in organic electronics. One of the most important is the charge-carrying properties of the organic material. For organic solar cells (OSC), the efficient transport of charges to the electrodes after exciton generation and charge separation is a key factor in determining device efficiency.[1] In bulk heterojunction (BHJ) solar cells, the electron and hole mobilities depend on the properties of the individual electron acceptor and donor materials and the phase separation between the two active layer components. After exciton formation and migration to a donor−acceptor interface, charge separation occurs. Electrons in the active layer move through regions rich in electron-acceptor material while holes migrate through the electron donor-rich phase. The active layer morphology is also an important determinant of solar cell efficiency. It should consist of a network of interpenetrating acceptor and donor-rich phases with domain size ideally in the range of 15 to 20 nm.[2] The crystallinity of the domains is also crucial to the overall charge mobility of the active layer. These two characteristics are common in both polymer and small molecule-based BHJ solar cells. A well-known example is the combination of poly(3-hexylthiophene) (P3HT) and [6,6]-phenyl-C61-butyric acid methyl ester ($PC_{61}BM$).[3] The $\pi-\pi$ interaction in the P3HT bulk material is essential for driving both the crystallinity of the P3HT domain and the phase separation from the $PC_{61}BM$ domain.

*To whom correspondence should be addressed. E-mail: wwhwong@unimelb.edu.au.

(1) Scharber, M. C.; Mühlbacher, D.; Koppe, M.; Denk, P.; Waldauf, C.; Heeger, A. J.; Brabec, C. J. *Adv. Mater.* **2006**, *18*, 789–794.
(2) Halls, J. J. M.; Pichler, K.; Friend, R. H.; Moratti, S. C.; Holmes, A. B. *Appl. Phys. Lett.* **1996**, *68*, 3120–3122.
(3) Dennler, G.; Scharber, M. C.; Brabec, C. J. *Adv. Mater.* **2009**, *21*, 1323–1338.

Published on Web 12/23/2009

In this study, hexa-*peri*-hexabenzocoronene (HBC) with a family of thiophene dendrons attached to its periphery was investigated as a self-organizing electron donor component in combination with fullerenes for BHJ solar cells.

HBC is a planar aromatic molecule consisting of 13 fused six-membered rings.[4,5] It belongs to a family of polycyclic aromatic hydrocarbons consisting of flat disk-like cores.[6] HBC and its derivatives have been shown to self-assemble into columnar structures giving rise to ordered morphology in films.[7,8] Mobility of 5×10^{-3} $cm^2\ V^{-1}\ s^{-1}$ was achieved in organic field effect transistors (OFET) using the self-assembling ability of a dodecyl-substituted HBC molecule.[9] There have only been limited reports on the use of HBC's in organic solar cells.[10−12] Currently, most HBC derivatives rely on alkyl chains on their periphery for solubility, which limits the potential for further functionalization.[4,13−15] It is also possible that these peripheral alkyl chains adversely affect charge separation at the donor−acceptor interface in the bulk heterojunction. Recently, we reported the synthesis and optoelectronic properties of highly soluble easily functionalized HBC building blocks carrying conjugated substituents.[16] The primary challenge in the synthesis of these systems is the incorporation of conjugated substituents as well as alkyl groups for solubility. From these studies, the 9,9-dioctylfluorenyl hexa-*peri*-hexabenzocoronene (FHBC) moiety has emerged as a material with excellent solubility and the potential for further derivatization.[16]

Thiophene-based compounds have emerged as one of the most important classes of materials in the area of organic electronics over the past decade.[17] From small molecules to polymers, these materials have been employed in a range of organic electronic devices, including organic light emitting diodes (OLED),[18−20] organic field effect transistors (OFET),[21,22] and organic solar cells (OSC).[3,23,24] This has been driven by their outstanding optical, redox, self-organizing, and charge-transport properties which can be easily tuned by chemical modification.[23,25,26] Recently, three-dimensional oligothiophene dendrimers have been revealed as viable hole transport materials in BHJ solar cells.[27−29] The design of these dendrimers allows creation of monodisperse materials with well-defined properties in contrast to conjugated polymers whose properties are to some extent chain-length dependent. These dendrimers can also be easily functionalized with a variety of dyes, redox-active centers, self-organizing moieties, or biologically active groups at their cores or peripheries.

With the benefits of self-organization in FHBCs and the outstanding tunable properties of thiophene-based oligomers, we set out to study hybrids containing both of these components. Here we report the synthesis and characterization of a series of thiophene dendrons attached to a central FHBC core. Evidence for the self-assembly of these hybrid materials in solution and in the solid state was observed. The performance of these novel FHBC-thiophene hybrids in BHJ solar cells was also investigated. The studies show good structure−property correlations and appropriately translate to BHJ solar cell performance.

Synthesis and Characterization

The synthesis of the FHBC core **1**[16] and the thiophene dendrons **4** and **5**[28] have been reported previously. The iodo substituents on the fluorene rings of FHBC **1** were removed using transmetalation with butyl lithium and protonation of the organolithium to give FHBC core **2** (Scheme 1). Suzuki−Miyaura coupling of the FHBC core **1** with the thiophene pinacol boronate esters **3**, **4**, and **5** gave, in excellent yields, the FHBC oligothiophene (FHBC−OT) hybrids **6**, **7**, and **9**, respectively, after purification by size exclusion chromatography (Scheme 1). The TMS groups of compounds **7** and **9** were removed by treatment with tetrabutylammonium fluoride which produced the desired FHBC−OT hybrids **8** and

(4) Wu, J.; Pisula, W.; Müllen, K. *Chem. Rev.* **2007**, *107*, 718–747.
(5) Herwig, P.; Kayser, C. W.; Müllen, K.; Spiess, H. W. *Adv. Mater.* **1996**, *8*, 510–513.
(6) Destrade, C.; Nguyen Huu, T.; Gasparoux, H.; Malthete, J.; Levelut, A. M. *Mol. Cryst. Liq. Cryst.* **1981**, *71*, 111–35.
(7) Ito, S.; Wehmeier, M.; Brand, J. D.; Kubel, C.; Epsch, R.; Rabe, J. P.; Müllen, K. *Chem.—Eur. J.* **2000**, *6*, 4327–4342.
(8) Kastler, M.; Pisula, W.; Wasserfallen, D.; Pakula, T.; Müllen, K. *J. Am. Chem. Soc.* **2005**, *127*, 4286–4296.
(9) Pisula, W.; Menon, A.; Stepputat, M.; Lieberwirth, I.; Kolb, U.; Tracz, A.; Sirringhaus, H.; Pakula, T.; Müllen, K. *Adv. Mater.* **2005**, *17*, 684–689.
(10) Schmidtke, J. P.; Friend, R. H.; Kastler, M.; Müllen, K. *J. Chem. Phys.* **2006**, *124*, 174704/1–174704/6.
(11) Schmidt-Mende, L.; Watson, M.; Müllen, K.; Friend, R. H. *Mol. Cryst. Liq. Cryst.* **2003**, *396*, 73–90.
(12) Schmidt-Mende, L.; Fechtenkotter, A.; Müllen, K.; Moons, E.; Friend, R. H.; MacKenzie, J. D. *Science* **2001**, *293*, 1119–1122.
(13) Wu, J.; Grimsdale, A. C.; Müllen, K. *J. Mater. Chem.* **2005**, *15*, 41–52.
(14) Yamamoto, Y.; Fukushima, T.; Suna, Y.; Ishii, N.; Saeki, A.; Seki, S.; Tagawa, S.; Taniguchi, M.; Kawai, T.; Aida, T. *Science* **2006**, *314*, 1761–1764.
(15) Hill, J. P.; Jin, W.; Kosaka, A.; Fukushima, T.; Ichihara, H.; Shimomura, T.; Ito, K.; Hashizume, T.; Ishii, N.; Aida, T. *Science* **2004**, *304*, 1481–1483.
(16) Wong, W. W. H.; Jones, D. J.; Yan, C.; Watkins, S. E.; King, S.; Haque, S. A.; Wen, X.; Ghiggino, K. P.; Holmes, A. B. *Org. Lett.* **2009**, *11*, 975–978.
(17) Mishra, A.; Ma, C.-Q.; Bäuerle, P. *Chem. Rev.* **2009**, *109*, 1141–1276.
(18) Perepichka, I. F.; Perepichka, D. F.; Meng, H.; Wudl, F. *Adv. Mater.* **2005**, *17*, 2281–2305.
(19) Grimsdale, A. C.; Leok Chan, K.; Martin, R. E.; Jokisz, P. G.; Holmes, A. B. *Chem. Rev.* **2009**, *109*, 897–1091.
(20) Mitschke, U.; Bäuerle, P. *J. Mater. Chem.* **2000**, *10*, 1471–1507.
(21) Ong, B. S.; Wu, Y.; Li, Y.; Liu, P.; Pan, H. *Chem.—Eur. J.* **2008**, *14*, 4766–4778.
(22) Allard, S.; Forster, M.; Souharce, B.; Thiem, H.; Scherf, U. *Angew. Chem., Int. Ed.* **2008**, *47*, 4070–4098.
(23) *Handbook of Oligo- and Polythiophenes*; Fichou, D., Ed.; Wiley-VCH: Weinheim, Germany, 1999.
(24) Li, Y.; Zou, Y. *Adv. Mater.* **2008**, *20*, 2952–2958.
(25) Roncali, J. *Chem. Rev.* **1997**, *97*, 173–205.
(26) Bäuerle, P. In *Electronic Materials: The Oligomer Approach*; Müllen, K., Wegner, G., Eds.; Wiley-VCH: Weinheim, Germany, 1998; p 105−197.
(27) Kopidakis, N.; Mitchell, W. J.; van de Lagemaat, J.; Ginley, D. S.; Rumbles, G.; Shaheen, S. E.; Rance, W. L. *Appl. Phys. Lett.* **2006**, *89*, 103524.
(28) Ma, C.-Q.; Mena-Osteritz, E.; Debaerdemaeker, T.; Wienk, M. M.; Janssen, R. A.; Bäuerle, P. *Angew. Chem., Int. Ed.* **2007**, *46*, 1679–1683.
(29) Ma, C.-Q.; Fonrodona, M.; Schikora, M. C.; Wienk, M. M.; Janssen, R. A. J.; Bäuerle, P. *Adv. Funct. Mater.* **2008**, *18*, 3323–3331.

Scheme 1. Synthesis of Fluorenyl Hexa-*peri*-hexabenzocoronene−Thiophene Hybrids [a]

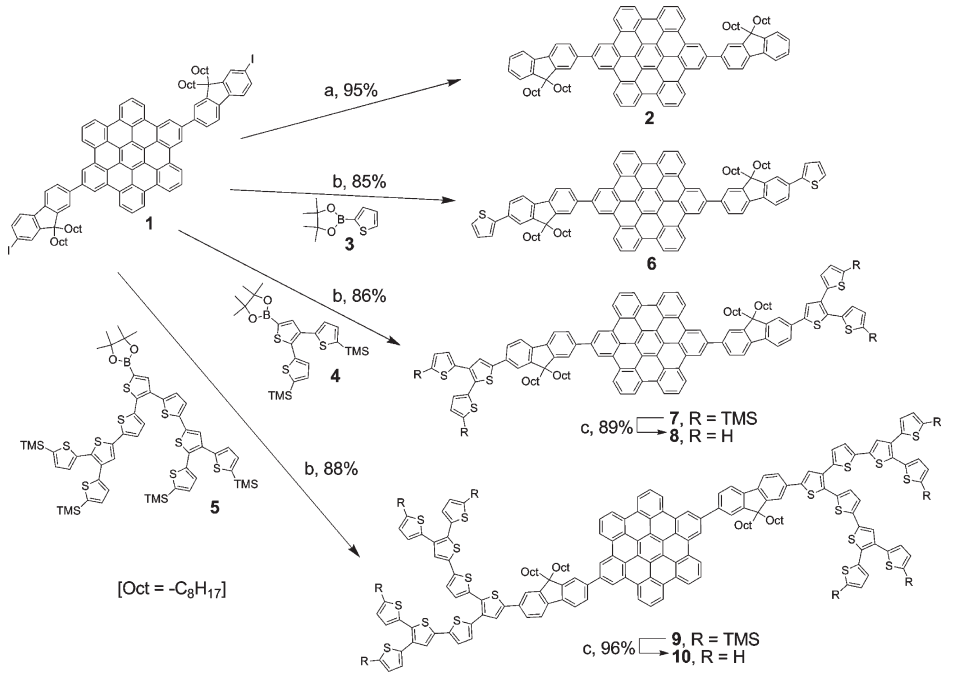

[a] Conditions: (a) n-BuLi, THF, −78 °C, 15 min, H_2O, −78 to 25 °C, 30 min; (b) $Pd(PPh_3)_4$, Et_4NOH (20% w/v aq), toluene, 90 °C, 14 h; (c) $Bu_4N^+F^-\cdot 3H_2O$, THF, 25 °C, 30 min.

10 in near quantitative yield (see Supporting Information for full details of characterization of all new compounds). All compounds were highly soluble in organic solvents and have good film forming properties, which is essential in the preparation of devices by solution deposition techniques.

Optoelectronic Properties

The optoelectronic properties of organic materials are important parameters that determine the applicability of a material in organic electronic devices. In bulk heterojunction solar cells, the UV−vis absorption profile of the material is very important, as it relates to the quantity of photons the device can potentially capture. Equally important are the relative energy levels of the electron donor and acceptor materials. The energy gap between the highest occupied molecular orbital (HOMO) of the donor and the lowest unoccupied molecular orbital (LUMO) of the acceptor defines the potential output (open circuit voltage) of the device.[3] In this study, the HOMO and LUMO energy levels of the materials were measured from a combination of UV−vis spectroscopic and electrochemical techniques.

The UV−vis spectra of FHBC core **2** and FHBC−OT hybrids **6**, **8**, and **10** in dichloromethane solution (10^{-5} M) are shown in Figure 1a. The absorption profiles of FHBC core **2** and hybrid **6** are very similar with absorption maxima at 364 and 367 nm, respectively. The UV−vis spectrum of **8** shows an increase in absorbance between 350 and 450 nm compared with **6**. However, no red-shift was observed either for the maximum absorption wavelength or the onset absorption wavelength, indicating a lack of π-conjugation between the thiophene units and the FHBC core. Increasing the peripheral thiophene dendron size from 6 thiophene units in compound **8** to 18 thiophene units in compound **10** resulted in an increased absorbance by the FHBC−OT system. The UV−vis absorption profile of **10** is red-shifted compared with **6** and **8**, with absorption onset at 500 nm. From the UV−vis data in solution, a HOMO−LUMO gap of 2.51 eV was obtained from for **10**, which agrees well with the energy gap of the second generation thiophene dendron **9T** at 2.67 eV (Figure 1b).[28] The fact that the second generation dendrimer **18T** has a more red-shifted absorption compared with that of the FHBC−OT hybrid **10** again indicates a lack of conjugation through the entire structure of compound **10** (Figure 1b). The break in conjugation is probably due to the relative conformation of the 9,9-dioctylfluorene units in relation to the hexa-*peri*-hexabenzocoronene core in compound **10**. Despite this observation, compound **10** has significantly higher molar absorptivity than either **9T** or **18T** which will prove advantageous in solar cell devices (Table 1). The UV−vis absorption profile of FHBC−OT hybrid **10** was recorded at a range of concentrations (Figure 1c). The relative intensities of the absorption bands change with concentration, suggesting a degree of molecular aggregation in solution. This concentration dependence of UV−vis spectra was also observed for compound **8** (see Supporting Information). UV−vis absorption of the thin films of all FHBC derivatives **2**, **6**, **8**, and **10** show a shift in absorption to longer wavelengths compared with their corresponding solution spectra (see Supporting Information). For example, the absorption onset of FHBC−OT hybrid **10** as a thin film is at 550 nm compared with an onset at 500 nm in solution (Figure 1a). This red-shift in absorption in solid state is indicative of

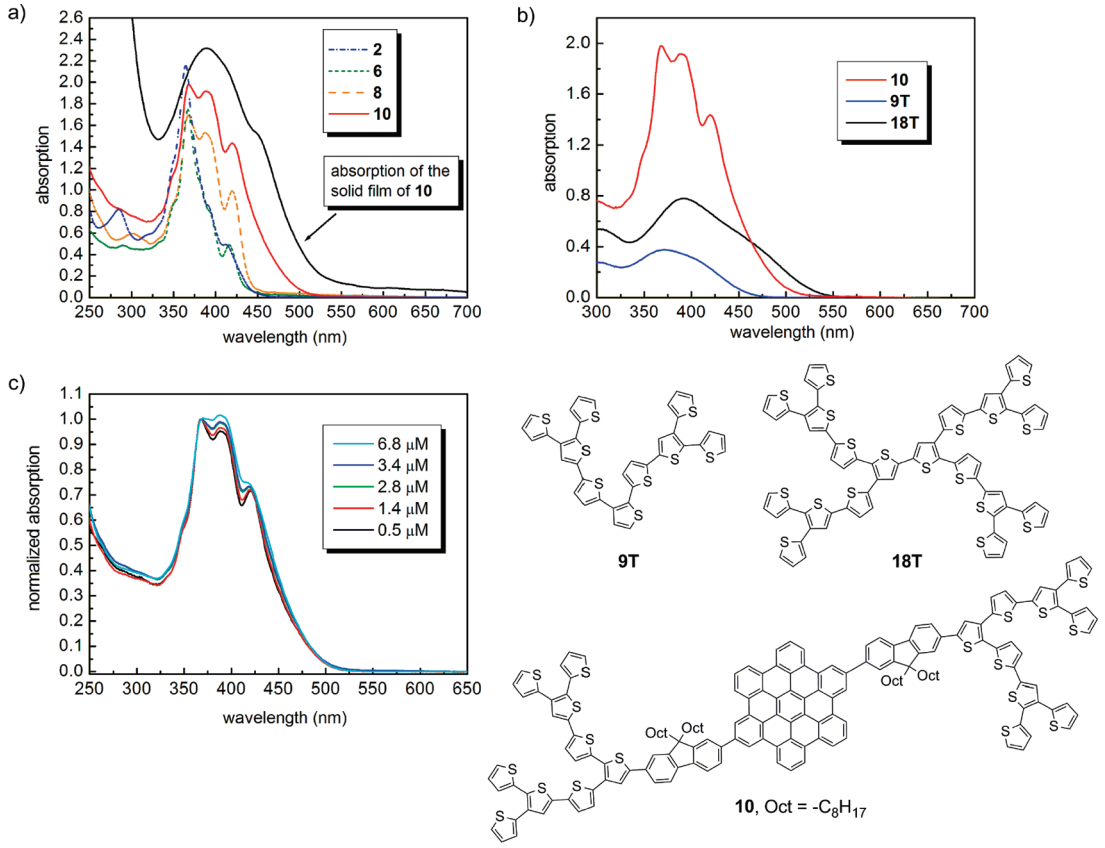

Figure 1. (a) UV−vis absorption spectra of FHBC derivatives **2**, **6**, **8**, and **10** (10^{-5} M in CH_2Cl_2) and the UV−vis absorption spectrum of a solid film of **10**; (b) UV−vis absorption spectra of FHBC−OT hybrid **10** and thiophene dendron **9T** and dendrimer **18T** in CH_2Cl_2 solution (10^{-5} M);[28] (c) normalized UV−vis spectra of compound **10** in CH_2Cl_2 solution at various concentrations.

Table 1. Optical and Redox Data of the FHBC Core 2 and HBC-OT Hybrid Compounds

compounds	λ_{abs}^{max} (nm)[a]	$\varepsilon \times 10^5$ (cm·L·mol^{-1})[a]	E_g^{opt} [eV] [a,b]	E_{ox}^{1} [V][c,d]	E_{ox}^{onset} [V][c]	HOMO [eV][e]	LUMO [eV][f]
2	364	2.15	2.87	0.24	0.23	−5.33 (−5.28)	−2.46
6	367	1.75	2.86	0.32	0.24	−5.34 (−5.37)	−2.48
7	367	1.71	2.79	0.31	0.22	−5.32 (−5.27)	−2.53
8	368	1.69	2.81	0.31	0.23	−5.33 (−5.38)	−2.52
9	367	2.17	2.47	0.24	0.22	−5.32 (−5.19)	−2.85
10	369	1.98	2.51	0.24	0.18	−5.28 (−5.40)	−2.77
9T	373	0.38	2.69	0.57	0.51	−5.61	−2.92
18T	392	0.78	2.35	0.46[g]	0.42[g]	−5.52[g]	−3.17

[a] In CH_2Cl_2, 1×10^{-5} M, 295 K. [b] Determined from the onset of absorption. [c] In CH_2Cl_2, 1×10^{-3} M, Bu_4NPF_6 (0.1 M), 295 K, scan rate = 100 mV·s^{-1}, versus Fc/Fc^+. [d] Determined by differential pulse voltammetry. [e] Determined from $E_{HOMO} = -(E_{ox}^{onset} + 5.10)$ (eV);[1] data in brackets measured by photoelectron spectroscopy in air.[30,31] [f] Calculated from LUMO = HOMO + E_g^{opt}. [g] In DMF, 1×10^{-4} M, Bu_4NPF_6 (0.1 M), 295 K, scan rate = 100 mV·s^{-1}, versus Fc/Fc^+.

aggregation in the solid state. The aggregation behavior of these FHBC derivatives will be examined in greater detail in the following section using NMR spectroscopy in solution and wide-angle X-ray scattering (WAXS) in solid state. Apart from increasing the UV−vis absorption profile, the aggregation of these compounds will have important effects on their solid state morphology. As mentioned in the introduction, morphology control in donor−acceptor blend films is crucial to the charge separation and charge transport processes that occur directly after photoexcitation in a bulk heterojunction solar cell device.

Electrochemical studies for FHBC core **2** and FHBC−OT hybrids **6**, **8**, and **10** were performed in dichloromethane solution. A summary of the electrochemical data can be found in Table 1 (see Supporting Information for cyclic and differential pulse voltammograms). Energy level diagrams of compounds **2**, **6**, **8**, and **10** derived from electrochemical and UV−vis absorption data are shown in Figure 2. The energy level information suggests all four FHBC derivatives are suitable candidates as electron donor materials in a bulk heterojunction solar cell with [6,6]-phenyl-C61-butyric acid methyl ester ($PC_{61}BM$) as the electron acceptor.[1] Energy or charge transfer between a donor and an acceptor material can be observed by fluorescence quenching studies. The quenching of the fluorescence of the FHBC derivatives by $PC_{61}BM$ is another indication of compatibility of the materials for use in BHJ solar cell devices. In thin films, the fluorescence of the FHBC derivatives was completely quenched

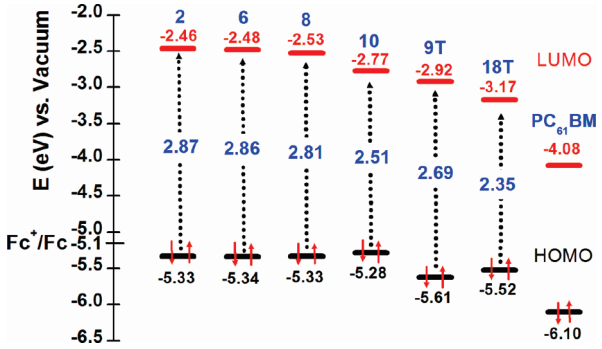

Figure 2. Energy level diagram of FHBC core **2** and FHBC−OT hybrids **6**, **8**, and **10**, thiophene dendrimers **9T** and **18T** and $PC_{61}BM$. The data were derived from CV and UV−vis absorption data. Note: $PC_{71}BM$ has a similar LUMO energy level to $PC_{61}BM$.[21].

when blended in a 1:2 weight ratio of FHBC to $PC_{61}BM$ (see Supporting Information).

Self-Association Properties and Solid State Morphology

As mentioned in the discussion of the UV−vis absorption experiments above, aggregation behavior was observed in solution and in the solid state. While many molecular systems will aggregate in solution given the appropriate solvation conditions, the ordered association of molecules requires correct molecular design. Planar aromatic systems, like hexa-*peri*-hexabenzocoronene (HBC), chiefly rely on $\pi-\pi$ stacking as the force for association. In fact, the poor solubility of unsubstituted HBC is a consequence of this strong $\pi-\pi$ stacking association. The fluorenyl HBC derivatives in this study rely on the 9,9-dioctylfluorene units to impart solubility. The steric bulk of the 9,9-dioctylfluorene groups limit extended aggregation compared with unsubstituted HBC. However, the 2,11-disubstitution arrangement on the HBC molecule with the fluorenyl groups as in compounds **2**, **6**, **8**, and **10** still allows $\pi-\pi$ stacking of the HBC core. This phenomenon can be directly observed by NMR spectroscopic studies in solution.

^{1}H NMR spectra of the aromatic region for compounds **2** and **8** at various concentrations are shown in Figure 3 (see Supporting Information for concentration dependence studies and fully assigned spectra for compounds **2**, **6**, **8**, and **10**). Peak assignments were made primarily on the basis of the multiplicity of the peaks and by comparison with spectra of known material. The ^{1}H NMR spectra of the FHBC core **2** and FHBC−OT hybrids **6**−**10** were found to be concentration dependent. It is clear that the protons assigned to the HBC core (H_{1-4}) shift upfield with increasing concentration (Figure 3). The protons on the fluorene moiety which are closest to the core (F_1 and F_3) also shift upfield with increasing concentration. The upfield shift of these protons is due to a shielding effect caused by staggered $\pi-\pi$ stacking between FHBC−OT molecules (Figures 3 and 4).[8,32] The fact that the protons on the thiophene moiety do not show changes in chemical shift as a function of concentration supports this staggered $\pi-\pi$ stacking model. An isodesmic model of indefinite stacking can be fitted to the changes in chemical shift with concentration.[33] Association constants (K) were obtained by fitting the data to the equation for isodesmic model for stacking with equal association constants.[33] The chemical shift of the H_1 proton of the unassociated monomer (δ_{mono}) was arbitrarily set at 9 ppm while that of the aggregate (δ_{aggre}) was arbitrarily set at 8 ppm. Plots of concentration versus chemical shift for compounds **2**, **6**, **8**, and **10** follow a similar trend and the data fit well ($R^2 > 0.99$, see Supporting Information for details of the nonlinear curve fit) with the proposed indefinite stacking model (Figure 4). It is interesting to note that the increase in thiophene dendron size does not appear to have an adverse effect on the proposed $\pi-\pi$ stacking association of the HBC core. In fact, there appears to be an increase in association with increasing dendron size. However, the significance of this observation is uncertain as the calculated deviation on the association constant is close to ±20% (see Supporting Information for nonlinear curve fit details). In any case, the results in these NMR studies support the observations made in the UV−vis spectroscopic studies confirming a self-association behavior in solution.

While the above-discussed NMR results indicate self-association in solution, X-ray scattering experiments provide information about the organization and phase formation in the solid state. Two-dimensional wide-angle X-ray scattering (2D-WAXS) experiments were performed on thin filaments of compounds **2**, **8**, and **10**. Filaments of 0.7 mm diameter were prepared by filament extrusion and mounted vertical toward the 2D detector. Figure 5a shows a 2D pattern for **2** which is characteristic for a discotic columnar liquid crystalline phase.[34,35] The equatorial reflections indicate an orientation of the columnar stacks along the fiber alignment direction. A hexagonal columnar arrangement with a unit cell of $a_{hex} = 2.48$ nm for **2** was determined from the relative reciprocal spacing of $1:\sqrt{3}:2$ of the scattering intensities. The distinct meridional reflections in the wide-angle region are attributed to the cofacial π-stacking distance of 0.35 nm between individual molecules within the column. Thereby, the discs are packed with their molecular planes perpendicular to the columnar axis as illustrated schematically in Figure 5a. This liquid crystalline organization remains unchanged over the whole investigated temperature range of −100 to 200 °C, and is in agreement with the thermal analysis by differential scanning calorimetry (DSC), which did not reveal any phase

(30) Kane, E. O. *Phys. Rev.* **1962**, *127*, 131–141.
(31) Kirihata, H.; Uda, M. *Rev. Sci. Instrum.* **1981**, *52*, 68–70.
(32) Wu, J.; Fechtenkotter, A.; Gauss, J.; Watson, M. D.; Kastler, M.; Fechtenkotter, C.; Wagner, M.; Müllen, K. *J. Am. Chem. Soc.* **2004**, *126*, 11311–11321.
(33) Martin, R. B. *Chem. Rev.* **1996**, *96*, 3043–3064.
(34) Laschat, S.; Baro, A.; Steinke, N.; Giesselmann, F.; Hägele, C.; Scalia, G.; Judele, R.; Kapatsina, E.; Sauer, S.; Schreivogel, A.; Tosoni, M. *Angew. Chem., Int. Ed.* **2007**, *46*, 4832–4887.
(35) Sergeyev, S.; Pisula, W.; Geerts, Y. H. *Chem. Soc. Rev.* **2007**, *36*, 1902–1929.

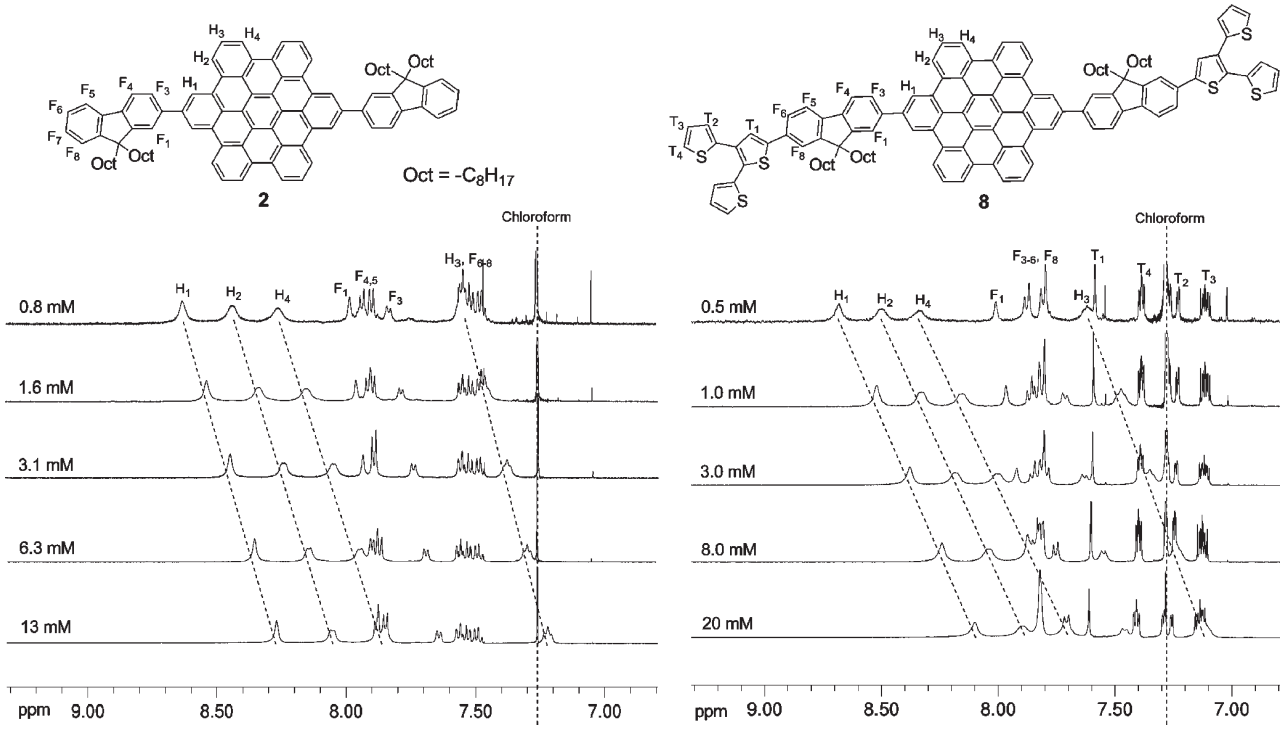

Figure 3. Concentration dependent ^{1}H NMR spectra of compounds **2** and **8** ($CDCl_3$ at 20 °C). Assignment of the spectra was primarily based on the multiplicity of the peaks and by comparison with spectra of known materials.

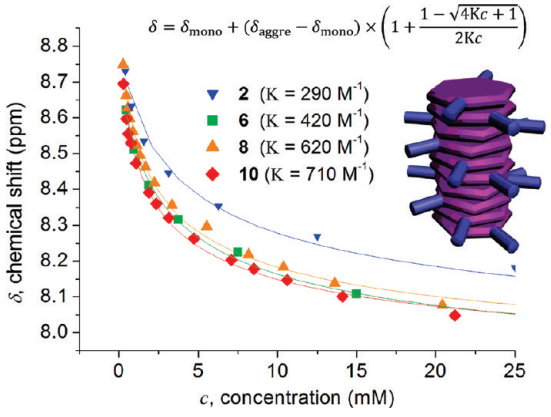

Figure 4. Variation in the ^{1}H NMR chemical shift of H_1 as a function of concentration for compounds **2**, **6**, **8**, and **10**. The equation is derived from the isodesmic model for stacking with equal association constants.[33]

transitions. Similarly, compound **8** showed no transitions in the DSC scans. The structural analysis for **8** pointed toward a rectangular columnar organization with unit cell dimensions of $a = 2.56$ and $b = 1.91$ nm. The significantly smaller unit cell in comparison to the theoretical molecular length (*ca.* 4.2 nm) is related to only two substituents (low density of the substitution mantel around the HBC stack) and thus intercalation of these substituents between neighboring columns. A π-stacking distance of 0.35 nm was also determined for **8** from the wide-angle meridional scattering intensity. In strong contrast to the behavior of FHBC **2**, the appearance of additional meridional reflections for compound **8** is characteristic of a complex helical packing of the molecules within the stacks.[36−41] The position of the middle-angle reflection indicated in Figure 5b is related to an additional period of 1.4 nm between every fourth molecule (1.4 nm/0.35 nm = 4) along the column possessing identical positional order. Thereby, the discs are substantially rotated by 45° to each other, while the aromatic HBC cores are perpendicular to the columnar axis. The additional meridional intensities at multiple scattering angles are higher order reflections. This kind of helical arrangement in a so-called plastic phase is in agreement with other discotic molecules bearing bulky substituents which induce a lateral rotation of neighboring discs.[42−49]

(36) Holst, H. C.; Pakula, T.; Meier, H. *Tetrahedron* **2004**, *60*, 6765–6775.
(37) Pisula, W.; Kastler, M.; Wasserfallen, D.; Robertson, J. W. F.; Nolde, F.; Kohl, C.; Muellen, K. *Angew. Chem., Int. Ed.* **2006**, *45*, 819–823.
(38) Livolant, F.; Levelut, A. M.; Doucet, J.; Benoit, J. P. *Nature* **1989**, *339*, 724–726.
(39) Percec, V.; Imam, M. R.; Peterca, M.; Wilson, D. A.; Heiney, P. A. *J. Am. Chem. Soc.* **2009**, *131*, 1294–1304.
(40) Peterca, M.; Percec, V.; Imam, M. R.; Leowanawat, P.; Morimitsu, K.; Heiney, P. A. *J. Am. Chem. Soc.* **2008**, *130*, 14840–14852.
(41) Lehmann, M.; Jahr, M.; Donnio, B.; Graf, R.; Gemming, S.; Popov, I. *Chem.—Eur. J.* **2008**, *14*, 3562–3576.
(42) Vera, F.; Serrano, J.-L.; Sierra, T. *Chem. Soc. Rev.* **2009**, *38*, 781–796.
(43) Barberá, J.; Cavero, E.; Lehmann, M.; Serrano, J.-L.; Sierra, T.; Vázquez, J. T. *J. Am. Chem. Soc.* **2003**, *125*, 4527–4533.
(44) Percec, V.; Imam, M. R.; Peterca, M.; Wilson, D. A.; Graf, R.; Spiess, H. W.; Balagurusamy, V. S. K.; Heiney, P. A. *J. Am. Chem. Soc.* **2009**, *131*, 7662–7677.
(45) Feng, X.; Wu, J.; Ai, M.; Pisula, W.; Zhi, L.; Rabe, J. P.; Müllen, K. *Angew. Chem., Int. Ed.* **2007**, *46*, 3033–3036.
(46) Pisula, W.; Tomović, Ž.; Watson, M. D.; Müllen, K.; Kussmann, J.; Ochsenfeld, C.; Metzroth, T.; Gauss, J. *J. Phys. Chem. B* **2007**, *111*, 7481–7487.
(47) Feng, X.; Pisula, W.; Müllen, K. *J. Am. Chem. Soc.* **2007**, *129*, 14116–14117.
(48) Feng, X.; Marcon, V.; Pisula, W.; Hansen Michael, R.; Kirkpatrick, J.; Grozema, F.; Andrienko, D.; Kremer, K.; Müllen, K. *Nat. Mater.* **2009**, *8*, 421–426.
(49) Fontes, E.; Heiney, P. A.; De Jeu, W. H. *Phys. Rev. Lett.* **1988**, *61*, 1202–1205.

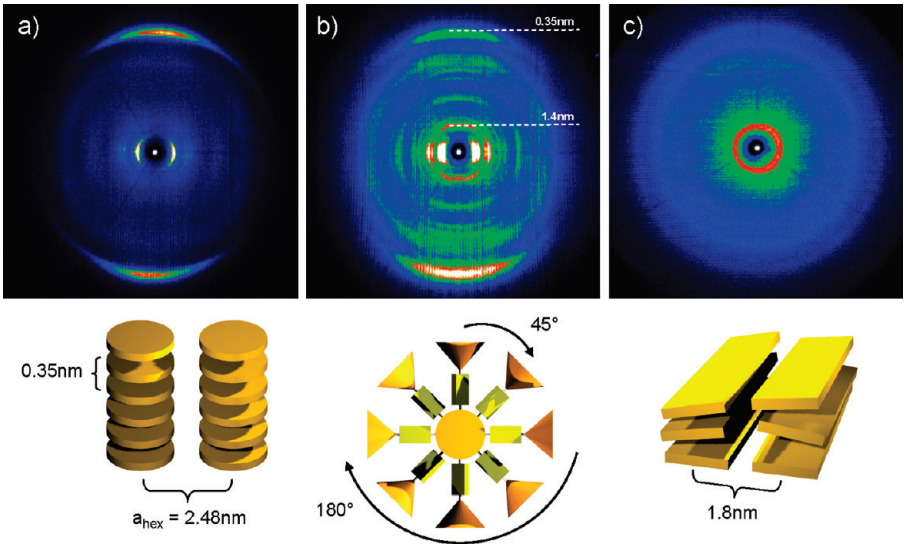

Figure 5. Fiber 2D-WAXS patterns of compounds (a) **2** and illustration of the discotic packing, (b) **8** and top view of the helical stack, (c) **10** and its disordered layer organization. The patterns were recorded at 30 °C.

Typically, such helical organization in liquid crystalline columnar stacks vanishes at high temperatures, but this complex arrangement for compound **8** remained unchanged at 160 °C indicating pronounced stability of the plastic phase within a broad temperature range. The direct comparison of the intracolumnar packing between **2** and **8** indicates that the helical stacking originates from the additional sterically demanding thiophene dendrons on compound **8**. The increase of the steric hindrance by attaching even larger **9T** dendrons for dendrimer **10** resulted in a more disordered structure in the bulk. The isotropic reflection corresponding to a distance of 1.8 nm is attributed to the spacing between lamellar layers which are formed by local phase separation between the rigid aromatic part and flexible side chains (Figure 5c). The molecules within the lamellar structures of **10** are much more disordered compared to the molecules in the columnar packing of FHBC **2** and **8**. These structural parameters are reflected in the BHJ solar cell performance characteristics of these materials and will be discussed in the following section.

The surface morphology of thin films was examined using tapping mode atomic force microscopy (AFM). The samples were prepared by spin-coating the material of interest on silicon substrate (25 mg/mL in chlorobenzene, 2000 rpm). The tapping mode AFM images of thin films of blends of compounds **2**, **6**, **8**, and **10** with $PC_{61}BM$ (1:2) are shown in Figure 6. Nanoscale phase separation was observed in all four blend films. The blend of **2** and $PC_{61}BM$ film gave the largest phase separation with domain sizes of ~100 nm (Figure 6a). The phase domains were smaller for blend films of **6**, **8**, and **10** with $PC_{61}BM$, and smoother film surfaces were observed. These differences in film morphology have consequences to device performance and will be discussed in the following section. Pristine films of compounds **2**, **6**, **8**, and **10** were also examined using tapping mode AFM (see Supporting Information for AFM images). The surface roughness of films containing compounds **2** and **8** was much higher than the roughness of the film containing compound **10**.

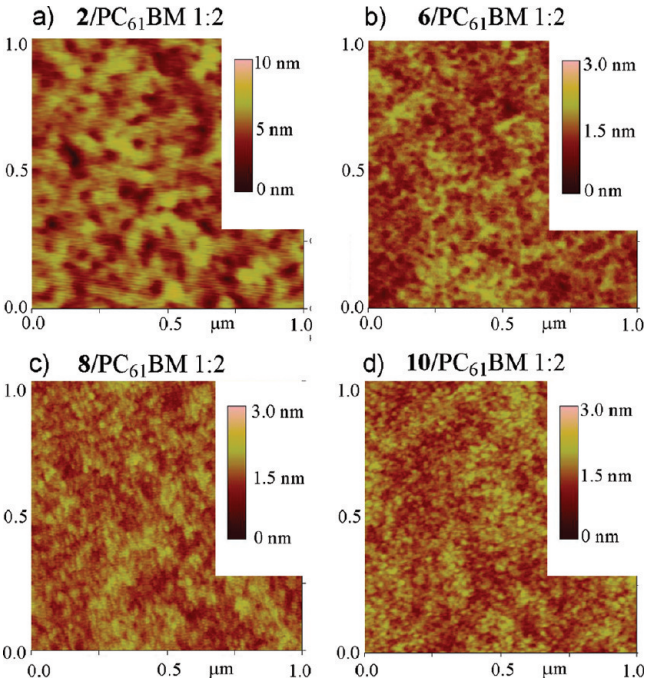

Figure 6. Morphology of blend films on silicon substrate spin-coated from chlorobenzene as imaged by tapping mode AFM: (a) compound **2**/$PC_{61}BM$ (1:2 weight ratio); (b) compound **6**/$PC_{61}BM$ (1:2 weight ratio); (c) compound **8**/$PC_{61}BM$ (1:2 weight ratio); and (d) compound **10**/$PC_{61}BM$ (1:2 weight ratio). The images ($1 \times 1\ \mu m^2$) display the surface topography (height in nm).

This is in agreement with the results obtained in the 2D-WAXS experiments where higher molecular order and crystallinity was observed for compounds **2** and **8** compared to compound **10** (Figure 5). In addition to the 2D-WAXS and AFM experiments, X-ray measurements were obtained for thin films of blends of the donor and acceptor materials. Thin films of compound **2** and $PC_{61}BM$ (1:2) were prepared by spin-coating chlorobenzene solutions of the blends on top of a PEDOT:PSS layer. This is the same as the solar cell device fabrication conditions (vide infra). After brief annealing (120 °C,

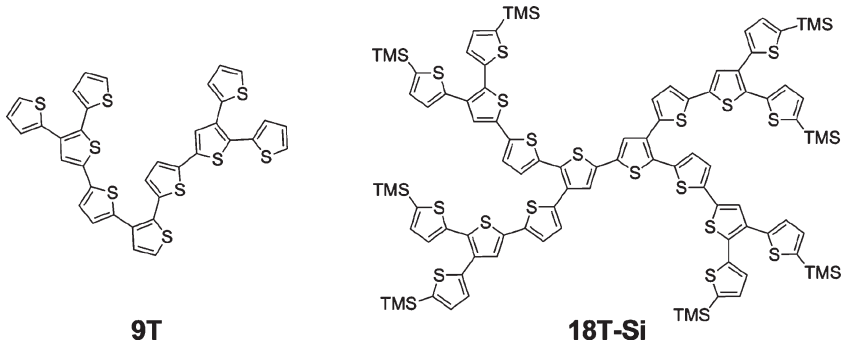

Figure 7. Structures of thiophene dendritic compounds[29] used as donor materials in BHJ solar cells for comparison with FHBC−OT hybrids.

5 min), a distinct reflection appeared which is indicative of supramolecular order in the blend (see Supporting Information, Figure S28). The reflections correspond to the hexagonal intercolumnar distance of compound **2** which was also observed for the neat donor material samples (see 2D WAXS in Figure 5a). In the thin film, the molecules are arranged on average in an edge-on fashion with the columnar axis parallel toward the substrate. These results indicate that the self-assembly of the FHBC compounds is not influenced by blending with $PC_{61}BM$, and phase separation between the donor and acceptor materials has to occur.

Bulk Heterojunction Solar Cells

Given all the photophysical and self-organization studies presented above, the FHBC derivatives appear ideal candidates to be employed as the electron donor material in BHJ solar cells. BHJ solar cells with device structure ITO|PEDOT:PSS|FHBC−OT:fullerene (1:2 w/w)|LiF/Al [ITO, indium tin oxide; PEDOT, poly(3,4-ethylenedioxythiophene); PSS, poly(styrenesulfonate)], using the FHBC−OT hybrids **6**, **8**, and **10** as electron donors and fullerene derivatives as electron acceptor, were fabricated and characterized. Devices with compound **2**, using Ca instead of LiF at the Al cathode, were also fabricated and tested. The ratio of donor and acceptor materials was device-optimized at 1:2 and is in line with the fluorescence quenching studies. The thickness of the photoactive layers was optimized for each of the donor−acceptor blends and was typically between 60 and 70 nm. In general, all devices showed good diode-like behavior in the dark and photovoltaic effects under simulated AM 1.5G illumination. Table 2 summarizes the device performance of the various solar cells and the following characteristic parameters are given: short-circuit currents (J_{sc}), open-circuit voltages (V_{oc}), fill factors (FF), and power-conversion efficiencies (η). For comparison, the PV performance data of the all-thiophene dendron **9T** and the dendrimer **18T-Si** are shown in Table 2 and have been reported previously.[29] The structures of these thiophene dendritic materials are shown in Figure 7. Devices containing **18T** could not be fabricated due to the low solubility of **18T** in commonly used solvents. It should be noted that the device-optimized weight ratio between donors **9T** and **18T-Si** and $PC_{61}BM$ was 1:4. The difference

Table 2. Device Performance of Bulk Heterojunction Solar Cells (See Text) with Active Layers Consisting of Dendrimer/Fullerene 1:2 Blends. Active Layer Thickness Was 60-70 nm and Device Area Was 0.167 cm^2

entry	donor	acceptor (weight ratio)	J_{sc}[a] (mA cm^{-2})	V_{oc} (V)	FF	η[b] (%)
1	**2**[c]	$PC_{61}BM$ (1:2)	1.87	0.9	0.54	0.9
2	**6**	$PC_{61}BM$ (1:2)	2.73	0.9	0.44	1.1
3	**8**	$PC_{61}BM$ (1:2)	2.91	1.0	0.42	1.2
4	**10**	$PC_{61}BM$ (1:2)	3.33	1.0	0.44	1.5
5	**10**	$PC_{71}BM$ (1:2)	6.37	1.0	0.38	2.5
6	**9T**[d]	$PC_{61}BM$ (1:4)	1.42	1.0	0.31	0.5
7	**18T-Si**[d]	$PC_{61}BM$ (1:4)	2.39	0.9	0.35	0.8

[a] Determined by convoluting the spectral response with the AM 1.5G spectrum (100 mW cm^{-2}). [b] $\eta = J_{sc} \times V_{oc} \times FF$. [c] Ca was used instead of LiF for this device. [d] From ref 29.

in device-optimized weight ratio between the FHBC and thiophene dendron-based devices can be related to the morphology of the device films. In the case of the thiophene dendrons **9T** and **18T-Si**, more $PC_{61}BM$ is required for optimal phase separation, leading to an interpenetrating network morphology required for efficient device operation. On the other hand, there is clear phase-separation between the donor and acceptor domains in FHBC/$PC_{61}BM$ (1:2 w/w) blends as observed in AFM experiments (Figure 6). The current density to voltage and external quantum efficiency curves for the BHJ devices are shown in Figure 8.

High open-circuit voltages (V_{oc}) of 0.9−1.0 V were observed for all compound combinations. The V_{oc} of a BHJ solar cell device depends primarily on the energy gap between donor HOMO and acceptor LUMO of the materials. Energy gaps of 1.2−1.3 eV, derived from Figure 2, are in agreement with the V_{oc} values measured for the devices. These V_{oc} values are also comparable to that of pure thiophene dendrimers **9T** and **18T-Si** recently reported[29] and are considerably better than the typical V_{oc} of P3HT:$PC_{61}BM$ BHJ solar cells (0.55−0.65 V).[50] A clear trend was observed for the short-circuit currents (J_{sc}) of the series of devices. The value of J_{sc} increased with the broadening of the optical absorption from the zero generation dendrimer **6** to the second generation dendrimer **10**. The short circuit current J_{sc} of a compound **10** based device (Table 2, entry 4) is much higher than that of the corresponding thiophene dendron **9T** (entry 6) and dendrimer **18T-Si** (entry 7). This is due to the much higher

(50) Ma, W.; Yang, C.; Gong, X.; Lee, K.; Heeger, A. J. *Adv. Funct. Mater.* **2005**, *15*, 1617–1622.

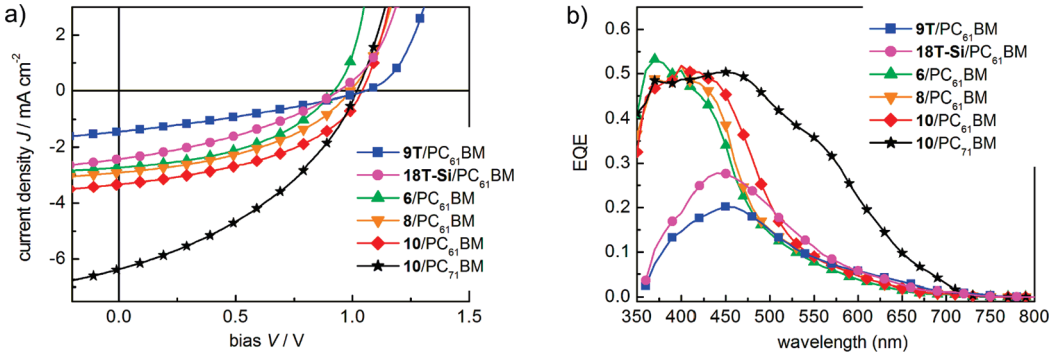

Figure 8. (a) $J-V$ curves and (b) EQE spectra of various active layer blends based devices.

absorption of **10** over 350−450 nm originating from the FHBC core (Figure 1b). In this study, the best fill factor (FF) of 0.54 was observed for the device containing the FHBC core **2**. A good FF indicates efficient as well as balanced charge transport within the active layer of the device. The ordered assembly of compound **2** in the solid state, as demonstrated by 2D-WAXS (Figure 5a), will almost certainly facilitate charge transport. The FF for the device containing **10** (entry 4) is higher than the **9T** and **18T-Si** devices (entry 6 and 7). This can be rationalized by the better charge carrier transport within the active layer induced by ordered assembly of the FHBC core moiety. The value of J_{sc} was also improved significantly by the use of $PC_{71}BM$ instead of $PC_{61}BM$ (compare entries 4 and 5 in Table 2).[51] $PC_{71}BM$ has increased optical absorption compared to $PC_{61}BM$ and has been shown to improve light harvesting in organic solar cells.[51] External quantum efficiency (EQE) spectra show the photocurrent response of the devices at wavelengths from 350 to 850 nm (Figure 8b). A maximum EQE of 50% was obtained for devices with $PC_{61}BM$ at around 400 nm. The maximum EQE of the device containing the FHBC−OT hybrid **10** and $PC_{71}BM$ was extended to 470 nm. A power conversion efficiency of 2.5% was achieved for the device with minimal optimization in the active layer thickness, donor−acceptor ratio, and morphology.

In summary, the addition of the FHBC core to the thiophene dendrimers has improved the performance of the material in BHJ solar cells. The FHBC core increased the photocurrent generated from the solar cells by absorbing more strongly over 350−450 nm compared to the pure thiophene dendrimers (Figures 1b and 8b). In addition, the self-assembling properties of the FHBC core drives the formation of ordered morphology in solid state. The 2D-WAXS experiments showed self-assembly of the FHBC material into ordered structures (Figure 5) while tapping mode AFM studies indicate nanoscale phase separation between the donor and acceptor domains in blend films (Figure 6). Ordered structures were also observed in X-ray measurements on blend films. This indicates the ordered structures in the donor FHBC domain are unaffected in their blends with $PC_{61}BM$ and phase separation between the donor and acceptor materials has occurred. The combination of nanoscale donor−acceptor phase separation and the formation of ordered structures within these domains are important to charge separation and transport in the active layer of the solar cells after photoexcitation. Studies are now in progress to examine the charge mobility in these BHJ solar cell devices using the photoinduced charge extraction by a linearly increasing voltage (photo-CELIV) technique.[52,53]

Conclusions

The design of novel materials for organic solar cell applications is currently a topic of great interest. While it is important to maximize the harvesting of sunlight by broadening the absorption profile of organic materials, it is also essential that the light energy absorbed by the material is efficiently converted into electric current. An interpenetrating network of donor and acceptor materials with domain size of 15−20 nm is thought to be ideal for charge separation and charge transport after photoexcitation in a bulk heterojunction (BHJ) solar cell device.[2] Molecular organization within the donor and acceptor domains is also important for charge transport. In this study, fluorenyl hexa-*peri*-hexabenzocoronene (FHBC) was employed as the scaffold for molecular organization. FHBC derivatives with various dendritic thiophene substituents have been shown to self-associate into ordered structures in solution and in solid state. BHJ solar cell devices fabricated with these compounds as electron donor materials show good performance achieving power conversion efficiency of 2.5%. In addition, a comparison of devices based on the FHBC derivatives and pure dendritic thiophene materials showed the positive effect of self-organization on device performance.

Acknowledgment. We thank the Australian Research Council (FF0348471, DP0451189, DP0877325) and the Commonwealth Scientific and Industrial Research Organization (CSIRO), the Victorian Government Department of

(51) Wienk, M. M.; Kroon, J. M.; Verhees, W. J. H.; Knol, J.; Hummelen, J. C.; van Hal, P. A.; Janssen, R. A. J. *Angew. Chem., Int. Ed.* **2003**, *42*, 3371–3375.

(52) Österbacka, R.; Pivrikas, A.; Juska, G.; Genevičius, K.; Arlauskas, K.; Stubb, H. *Curr. Appl. Phys.* **2004**, *4*, 534–538.

(53) Mozer, A. J.; Sariciftci, N. S.; Lutsen, L.; Vanderzande, D.; Österbacka, R.; Westerling, M.; Juska, G. *Appl. Phys. Lett* **2005**, *86*, 112104.

Primary Industries (VICOSC), the Victorian Endowment for Science, Knowledge and Innovation (VESKI), University of Melbourne, DAAD/Go8 exchange scheme, the Fonds der Chemischen Industrie, Deutsche Forschungsgemeinschaft (SFB 569) and the NAIMO EU integrated project (NMP4-CT-2004-500355) for generous financial support. We also thank Dr. Scott Watkins (CSIRO) for the use of the AC2 spectroscope for acquiring the photoelectron spectrum of the FHBC compounds in air.

Supporting Information Available: Experimental procedures, spectroscopic analytical data for all new compounds and details on device fabrication and measurement. This material is available free of charge via the Internet at http://pubs.acs.org.